Role of Changes in Mean Temperatures versus Temperature Gradients in the Recent Widening of the Hadley Circulation

ORI ADAM

Department of Earth Sciences, Eidgenössische Technische Hochschule Zürich, Zurich, Switzerland

TAPIO SCHNEIDER

Department of Earth Sciences, Eidgenossische Technische Hochschule Zürich, Zurich, Switzerland, and California Institute of Technology, Pasadena, California

NILI HARNIK

Department of Geosciences, Tel Aviv University, Tel Aviv, Israel

(Manuscript received 21 February 2014, in final form 17 June 2014)

ABSTRACT

The Hadley circulation (HC) has widened in recent decades, and it widens as the climate warms in simulations. But the mechanisms responsible for the widening remain unclear, and the widening in simulations is generally smaller than observed.

To identify mechanisms responsible for the HC widening and for model–observation discrepancies, this study analyzes how interannual variations of tropical-mean temperatures and meridional temperature gradients influence the HC width. Changes in mean temperatures are part of any global warming signal, whereas changes in temperature gradients are primarily associated with ENSO. Within this study, 6 reanalysis datasets, 22 Atmospheric Modeling Intercomparison Project (AMIP) simulations, and 11 historical simulations from phase 5 of the Climate Modeling Intercomparison Project (CMIP5) are analyzed, covering the years 1979–2012. It is found that the HC widens as mean temperatures increase or as temperature gradients weaken in most reanalyses and climate models. On average, climate models exhibit a smaller sensitivity of HC width to changes in mean temperatures and temperature gradients than do reanalyses. However, the sensitivities differ substantially among reanalyses, rendering the HC response to mean temperatures in climate models not statistically different from that in reanalyses.

While global-mean temperatures did not increase substantially between 1997 and 2012, the HC continued to widen in most reanalyses. The analysis here suggests that the HC widening from 1979 to 1997 is primarily the result of global warming, whereas the widening of the HC from 1997 to 2012 is associated with increased midlatitude temperatures and hence reduced temperature gradients during this period.

1. Introduction

The Hadley circulation (HC) has widened in recent decades, leading to an expansion of the subtropical dry zones (Hu and Fu 2007; Johanson and Fu 2009; Seidel and Randel 2007; Lucas et al. 2014; Cubasch et al. 2013; Nguyen et al. 2013). Climate models of phase 3 (Johanson and Fu 2009) and phase 5 (Ceppi and Hartmann 2013) of the Climate Model Intercomparison Project (CMIP3 and CMIP5) underestimate the widening, reinforcing speculations about the reliability of models and reanalyses (Johanson and Fu 2009; Quan et al. 2014) and of HC extent diagnostics (Davis and Rosenlof 2012).

The relative roles of global warming and of other climate variations in the recent widening of the HC are unclear. In idealized and comprehensive climate simulations, the total HC width (HCW; defined as the latitudinal distance between the northern and southern termini of the HC) increases on average by ~1.2° latitude per kelvin global surface temperature increase ($^\circ K^{-1}$) (Lu et al. 2007). Yet observations indicate that the HCW has increased at a substantially larger rate of up to ~7° K^{-1} (depending on the reanalysis used and the definition of HCW) between 1979 and 2005 (Johanson and Fu 2009).

Corresponding author address: Ori Adam, Department of Earth Sciences, ETH Zürich, Sonneggstrasse 5, 8092 Zurich, Switzerland. E-mail: ori.adam@live.com

DOI: 10.1175/JCLI-D-14-00140.1

Additionally, global warming—indicated by the positive trend in global-mean surface temperature—appears to have ''paused'' between 1997 and 2012 (Cubasch et al. 2013). Yet here we show that the widening of the HC has continued during that time.

The goal of the present paper is to identify factors that play a role in the observed and simulated widening of the HC and to assess their relative importance in observations and models so that possible causes of model biases can be pinpointed. Starting from the observation that El Niño and the Southern Oscillation (ENSO) are associated with substantial changes in HCW—the HC narrows during El Niño and widens during La Niña (Seager et al. 2003; Nguyen et al. 2013)—we define simple indices that decompose sea surface temperature (SST) variations orthogonally into factors that are primarily associated with global warming (mean SST changes) and ENSO (SST gradient changes).

We compare interannual variability and trends of the Hadley circulation width in 6 reanalysis datasets with 22 Atmospheric Model Intercomparison Project (AMIP) simulations, in which atmospheric GCMs are driven by prescribed historical SST, and with 11 CMIP5 historical simulations, in which coupled ocean–atmosphere GCMs are driven by prescribed historical atmospheric compositions (e.g., greenhouse gases and volcanic aerosols). This allows us to separate HCW trends owing to different factors; effects of recent changes in atmospheric composition, which should be captured in both AMIP and CMIP5 simulations, can be separated from the effects of recent changes in ocean conditions not related to external forcings (e.g., ENSO), which would be captured in AMIP but not necessarily in CMIP5 simulations.

2. Data

Annual-mean data derived from monthly means for the years 1979–2012 were analyzed from the six reanalysis datasets listed and expanded in Table 1 (with the exception of the Twentieth Century Reanalysis Project, for which only data through 2011 were available). Sea surface temperature and the Oceanic Niño Index (ONI, the deviation of the 3-month running mean SST from a moving 30-yr climatology in the Niño 3.4 region) were obtained from the extended reconstructed SST, version 3b (ERSST v3b) provided by the National Oceanic and Atmospheric Administration's National Climatic Data Center (Smith et al. 2008). Global surface temperature anomalies were obtained from the National Aeronautics and Space Administration's (NASA) Goddard Institute for Space Studies Surface Temperature Analysis (GISTEMP; Hansen and Lebedeff 1987), in which ERSST v3b is used for SST anomalies.

CMIP5 and AMIP monthly simulation data were downloaded from the Earth System Grid Federation (ESGF). A total of 22 AMIP and 11 CMIP5 simulations are used, covering the periods 1979–2008 and 1979–2005, respectively. Only the first ensemble run is analyzed for each model simulation. Model information is listed in Table 1. Additional information is available at the CMIP website (http://cmip-pcmdi.llnl.gov).

3. Results

The dominant interannual SST variations are associated with global warming and ENSO. Figure 1a shows the first (solid red) and second (solid blue) EOFs of zonally averaged interannual SST variations around their long-term mean for the years 1979–2012. For the principal component analysis, annual- and zonal-mean SSTs are computed from monthly SST variations around their long-term monthly mean. Variances and covariances are area weighted. The associated principal components account for 42% and 25% of the variance of the annual- and zonal-mean SSTs (Fig. 1b), respectively. It is evident from the structure of the EOFs and of the principal component time series (Fig. 1b) that the first EOF represents a global warming signal, and the second is associated with ENSO (this is also confirmed by comparing the second EOF with the leading EOF of the residual of the regression of the SST time series versus the overall mean temperature—not shown). Indeed, the SST difference between typical El Niño and La Niña conditions resembles the second EOF (Fig. 1a), and the associated principal component time series correlates strongly with ONI (Fig. 1b). The principal way in which ENSO variations manifest themselves in SST are changes in the meridional SST contrast between the tropics and midlatitudes.

The dominant interannual SST variations motivate a decomposition of SST variations into two simple orthogonal components: one associated with large-scale temperature changes and one associated with changes in meridional temperature contrasts between the tropics and midlatitudes. We define the indices Mean(SST) and Grad(SST) as the area-weighted mean SST anomaly between ±45° (total shaded area in Fig. 1a) and the difference between the mean SST anomaly between 20° and 45° in both hemispheres (dark shaded area) and the mean SST anomaly between ±20° (light shaded area in Fig. 1a). This choice of latitude belts is motivated by the structure of the second (ENSO) EOF, showing contrasting SST variations between ±20° and midlatitudes. The 0°–20° and 20°–45° latitude belts are approximately of equal area, making Mean(SST) and Grad(SST) approximately orthogonal. Sensitivity of the results to variation of the latitude separating the tropical and

TABLE 1. Reanalysis datasets and AMIP and CMIP5 climate simulations used in this study. Resolutions are given as number of latitude × longitude grid points or spectral truncation multiplied by the number of vertical levels. In the models' names, LR and MR refer to low and medium resolutions, and (A), (H), and (A/H) refer to AMIP, historical, and both AMIP and historical climate simulations, respectively.

Source	Description	Resolution
Reanalysis		
NCEP-I	NCEP–National Center for Atmospheric Research (NCEP–NCAR) Global Reanalysis I (Kalnay et al. 1996)	T62 × 28
NCEP-II	NCEP–Department of Energy Global Reanalysis II (Kanamitsu et al. 2002)	T62 × 28
ERA-Interim	European Center for Medium-Range Weather Forecasts (ECMWF) Interim Reanalysis (Dee et al. 2011)	T225 × 60
MERRA	NASA Modern-Era Retrospective Analysis for Research and Applications (Rienecker et al. 2011)	720 × 270 × 72
Twentieth Century Reanalysis	National Oceanic and Atmospheric Administration (NOAA)–Cooperative Institute for Research in Environmental Sciences Twentieth-Century Reanalysis VII (Compo et al. 2011)	T62 × 28
CFSR	NCEP Climate Forecast System Reanalysis (Saha et al. 2010)	T382 × 64
Climate Model		
BCC_CSM1.1(A/H)	Beijing Climate Center, Climate System Model, version 1.1	T42 × 26
BNU-ESM(A)	Beijing Normal University–Earth System Model	T42 × 26
CanAM4(A)	Fourth Generation Canadian Atmospheric Climate Model	T63 × 35
CanCM4(H)	Fourth Generation Canadian Coupled Global Climate Model	T63 × 35
CanESM2(H)	Second Generation Canadian Earth System Model	T63 × 35
CCSM4(A/H)	Community Climate System Model, version 4.0	288 × 192 × 26
CMCC-CM(A)	Centro Euro-Mediterraneo sui Cambiamenti Climatici Climate Model	T159 × 31
CSIRO Mk3.6.0(A)	Commonwealth Scientific and Industrial Research Organization Mark 3.6.0	T63 × 18
EC-EARTH(A)	EC-Earth Consortium	T159 × 62
FGOALS-g2.0(A)	Flexible Global Ocean–Atmosphere–Land System Model, gridpoint, version 2.0	T42 × 26
GFDL CM2.1(H)	Geophysical Fluid Dynamics Laboratory (GFDL) Climate Model, version 2.1	144 × 90 × 24
GFDL CM3(A/H)	GFDL Climate Model, version 3	144 × 90 × 48
GFDL-ESM2G(H)	GFDL Earth System Model with Generalized Ocean Layer Dynamics (GOLD) component	144 × 90 × 24
GFDL-ESM2M(H)	GFDL Earth System Model with Modular Ocean Model 4 (MOM4) component	144 × 90 × 24
GFDL-HiRAM-180(A)	GFDL High Resolution Atmospheric Model	576 × 360 × 17
GFDL-HiRAM-360(A)	GFDL High Resolution Atmospheric Model	1152 × 720 × 17
GISS-E2-H-CC(H)	Goddard Institute for Space Studies (GISS) Model E, coupled with HYCOM ocean model	180 × 73 × 40
GISS-E2-R(A/H)	GISS Model E, coupled with the Russell ocean model	144 × 90 × 40
GISS-E2-R-CC(H)	GISS Model E, coupled with the Russell ocean model	180 × 73 × 40
HadGEM2(A)	Hadley Centre Global Environmental Model, version 2	192 × 145 × 40
INM-CM4(A)	Institute of Numerical Mathematics Coupled Model, version 4.0	180 × 120 × 21
IPSL-CM5A-LR(A)	L'Institut Pierre-Simon Laplace Coupled Model, version 5A, coupled with NEMO	96 × 96 × 39
IPSL-CM5A-MR(A)	L'Institut Pierre-Simon Laplace Coupled Model, version 5A, coupled with NEMO	144 × 143 × 39
IPSL-CM5B-LR(A)	L'Institut Pierre-Simon Laplace Coupled Model, version 5B, coupled with NEMO	96 × 96 × 39
MPI-ESM-LR(A)	Max Planck Institute Earth System Model	T63 × 47
MPI-ESM-MR(A)	Max Planck Institute Earth System Model	T63 × 95
MRI-AGCM3.2H(A)	Meteorological Research Institute Atmospheric General Circulation Model, version 3.2	T319 × 64
MRI-CGCM3(A)	Meteorological Research Institute Coupled Atmosphere–Ocean General Circulation Model, version 3	T159 × 48
NorESM1-M(A)	Norwegian Earth System Model, version 1	144 × 96 × 26

midlatitude belts between 18° and 25° was weak, suggesting that the relevance of these indices is not restricted to present-day conditions.

Our choice of signs implies that Grad(SST) increases (becomes less negative) when midlatitudes warm, relative to the tropics, so it is negative during El Niño and positive during La Niña. The advantage of this sign convention is that HCW is expected to increase as either Mean(SST) or Grad(SST) increase, implying positive sensitivities of HCW with respect to either index.

Figure 2 shows the time series of annually averaged Mean(SST) (top, solid green) and Grad(SST) (bottom, solid blue) for the years 1979–2012. The trends of these indices during the periods 1979–97 and 1997–2012 are shown by solid gray lines, with gray shadings marking Studentized 95% confidence bounds. Note that the

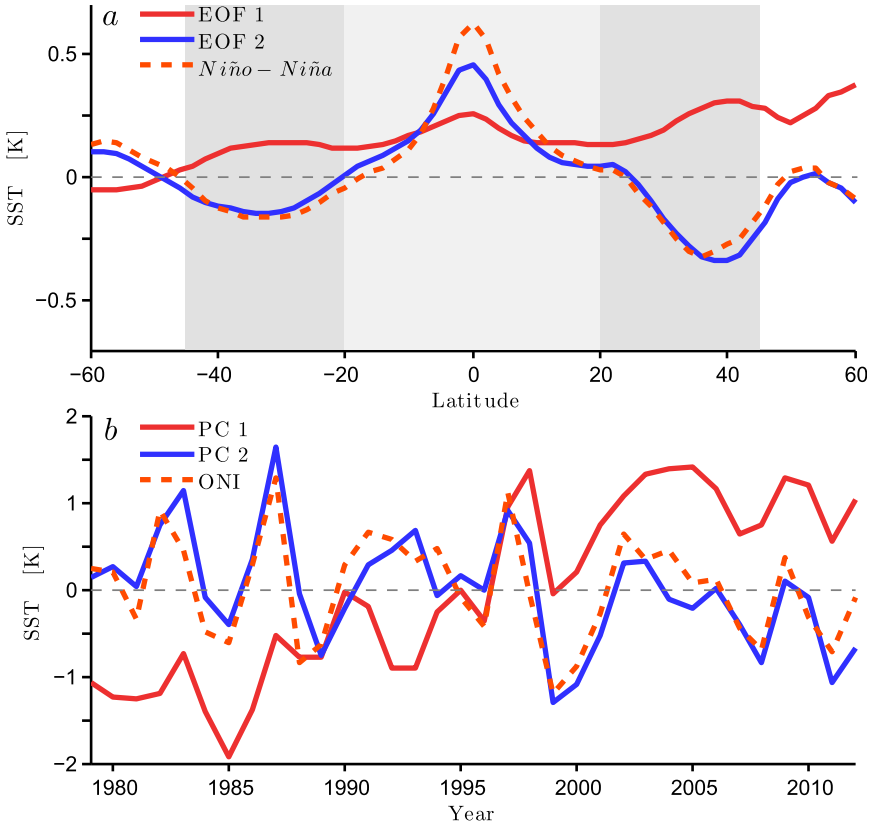

FIG. 1. EOFs and principal components (PC) of SST variations and SST variations associated with ENSO. (a) First (solid red) and second (solid blue) EOFs of zonal- and annual-mean SST variations and difference between composite El Niño and La Niña conditions (orange dashed) for the years 1979–2012 (ERSST v3b). Here, El Niño (La Niña) conditions are defined as ONI values greater (smaller) than 0.5 (−0.5). The normalized EOFs are multiplied by a factor of 2 K to match approximately the amplitude of the SST composite of typical El Niño − La Niña SST conditions. (b) Principal component time series associated with the first and second EOF (solid red and blue, respectively) and ONI (orange dashed).

dominance of the trend during the period 1979–97 introduces autocorrelation in the SST time series, which reduces the effective number of degrees of freedom. The effective confidence bounds during this period are therefore expected to be larger than those shown.

The overall (land–ocean) mean surface temperature anomaly (dashed magenta; GISTEMP) for the same period and latitude belt as Mean(SST) is shown for reference in the top panel. It is clear that Mean(SST) correlates strongly with the overall-mean surface temperature variations, but the inclusion of land areas in the temperature variations increases their variance. The ONI (dashed orange, multiplied by −1) is shown for reference in the bottom panel. As expected, Grad(SST) correlates strongly with ONI, with a (Pearson) correlation coefficient of −0.8.

To establish how the SST variations relate to HC variations, we define the terminus of the HC as the first latitude where the meridional mass streamfunction, averaged between the 850- and 300-hPa levels, changes sign poleward of the tropical extrema. The vertical averaging of the streamfunction reduces sensitivity to vertical structure (Kang et al. 2013; Davis and Birner 2013). The resulting HCW (latitudinal distance between the northern and southern termini of the HC) has relatively small intermodel variability (e.g., Johanson and Fu 2009; Quan et al. 2014; Nguyen et al. 2013) but may disagree with other extent indices (Davis and Rosenlof 2012; Davis and Birner 2013). This index is preferred here over other extent indices because it can be directly related to the dynamics at the HC terminus, as discussed in the following section.

The top panel of Fig. 3 shows the time series of the annual-mean HCW from the six reanalyses for the years 1979–2011. The northern and southern HC termini are shown separately in the bottom panel. The HC widening

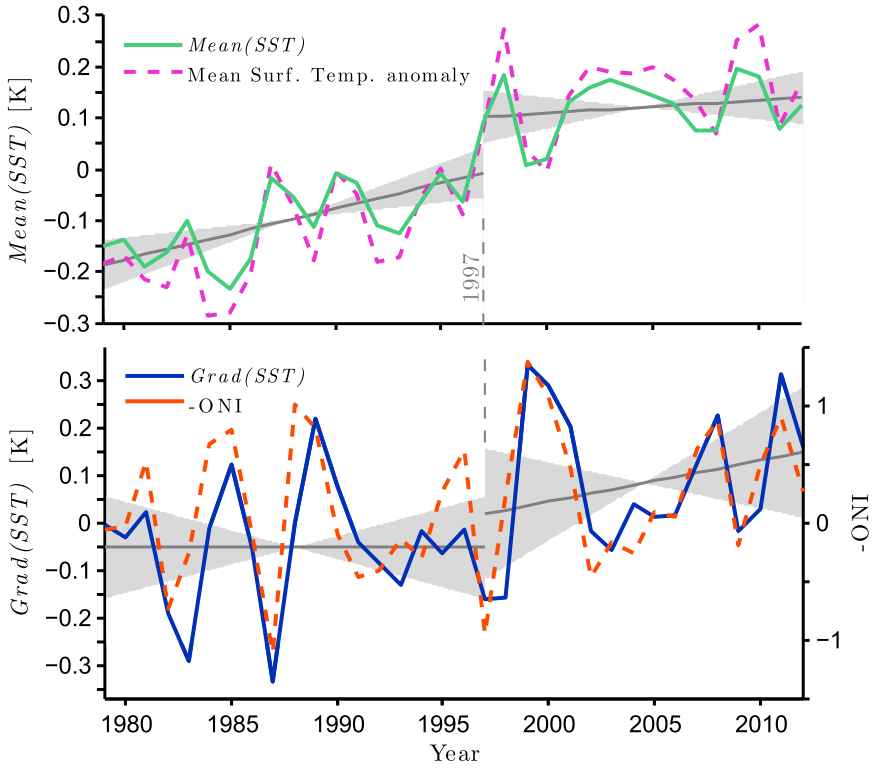

FIG. 2. (top) Time series of Mean(SST) (solid green) and overall-mean (land–ocean) surface temperature anomaly averaged between ±45° latitude (dashed magenta; GISTEMP) for the years 1979–2012. The Mean(SST) trends (solid gray) with 95% confidence bounds (shading) are shown for the periods 1979–1997 (0.1 ± 0.054 K decade^{-1}), and 1997–2012 (dark gray; 0.025 ± 0.068 K decade^{-1}). The mean value of Mean(SST) is 296.1 K (23°C). (bottom) Time series of Grad(SST) (solid blue; left vertical axis) and ONI (dashed orange; multiplied by −1; right vertical axis). The (Pearson) correlation coefficient between ONI and Grad(SST) is −0.8. The Grad(SST) trends (solid gray) with 95% confidence bounds (shading) are shown for the periods 1979–97 (0 ± 0.12 K decade^{-1}) and 1997–2012 (0.086 ± 0.18 K decade^{-1}). The mean value of Grad(SST) is −7.8 K.

is predominantly due to the poleward migration of the HC terminus in the Northern Hemisphere (Hu and Fu 2007), where the latitude of the terminus is also more variable than in the Southern Hemisphere. The standard deviation of the spread of HCWs across the reanalyses is 0.2°, increasing with time at a statistically significant ($p <$ 0.05) rate of 30% per decade.

Figure 4 shows trends in HC extent in the Southern Hemisphere (left column) and Northern Hemisphere (right column) over the years 1979–2005 for the 6 reanalyses (orange triangles), for the 22 AMIP simulations (blue crosses), and for the 11 CMIP5 simulations (green dots) listed in Table 1. Error bars mark Studentized 95% confidence bounds. Trends of ensemble means over reanalyses and simulations are shown without error bars. We note that AMIP trends in the Northern Hemisphere are weaker than those found by Allen et al. (2014), most likely because of differences in model ensembles.

The spread in trends across reanalyses is much higher than that across models, both in AMIP and CMIP5 simulations (Quan et al. 2014). Latest-generation reanalyses (ERA-Interim, MERRA, and CFSR) exhibit, on average, smaller trends than those shown by the first- and second-generation National Centers for Environmental Prediction (NCEP) reanalyses. The Twentieth-Century (20C) Reanalysis assimilates a more restricted subset of surface data and exhibits trends close to those of the NCEP reanalyses. These trends are substantially larger than those found in AMIP models, even though, like AMIP models, the 20C Reanalysis is forced by surface conditions.

We calculate the sensitivity of HCW to variations in Mean(SST) and Grad(SST) for each simulation by linearly regressing HCW against the SST indices. The regression analysis is restricted to annual means so that any subannual lag between SST variations and the HC

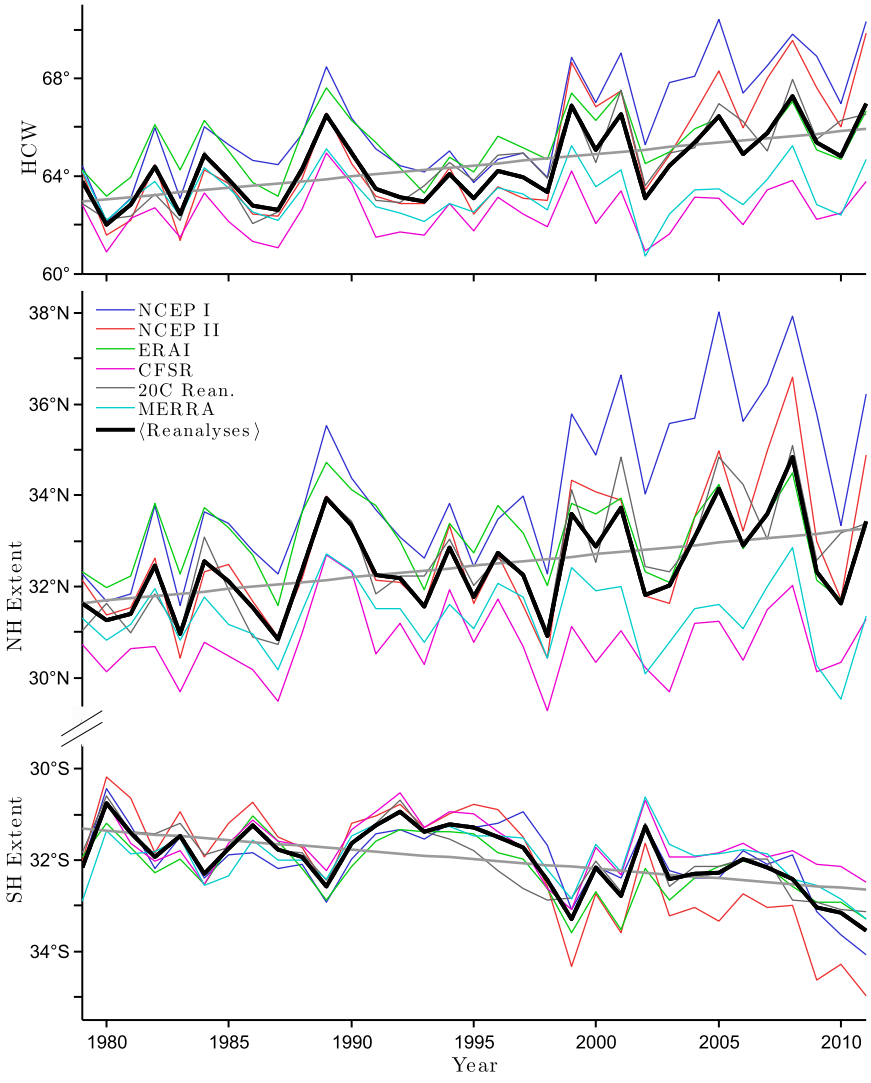

FIG. 3. (top) Time series (1979–2011) of the annually averaged HCW for the six reanalyses. Thick black and gray lines show ensemble means and linear trends ($0.93° \pm 0.43°$ decade^{-1}), respectively. (bottom) Time series of the HC extent with linear trend in the Northern Hemisphere ($0.51° \pm 0.33°$ decade^{-1}) and Southern Hemisphere ($-0.42° \pm 0.21°$ decade^{-1}) separately. The vertical axis is truncated for compactness. The spread of HCW across models has a standard deviation of 0.2°, which increases with time at a statistically significant ($p < 0.05$) rate of 30% per decade.

does not affect the results (Kang and Lu 2012; Davis and Birner 2013). The regression model is

$$\mathrm{HCW} = a_0 + a_1 \mathrm{Mean(SST)} + a_2 \mathrm{Grad(SST)} + \varepsilon,$$

where the coefficients a_1 and a_2 represent the sensitivity of the HCW to variations in Mean(SST) and Grad(SST), a_0 is an intercept, and ε is a residual.

Figure 5 shows the sensitivities for each reanalysis and simulation (with error bars marking Studentized 95% confidence bounds) calculated using the longest available period in each dataset [1979–2012 for reanalyses (orange triangles), 1979–2008 for AMIP simulations (blue crosses), and 1979–2005 for CMIP5 simulations (green dots)]. These sensitivities do not change substantially if the period of overlap among the datasets, 1979–2005, is used for AMIP simulations and reanalyses.

The sensitivities to Mean(SST) vary considerably across reanalyses. The NCEP I, NCEP II, and 20C reanalyses show statistically significant ($p < 0.05$) positive sensitivities, indicating that the HC widens as Mean(SST) increases. By contrast, the latest-generation reanalyses (ERA-Interim,

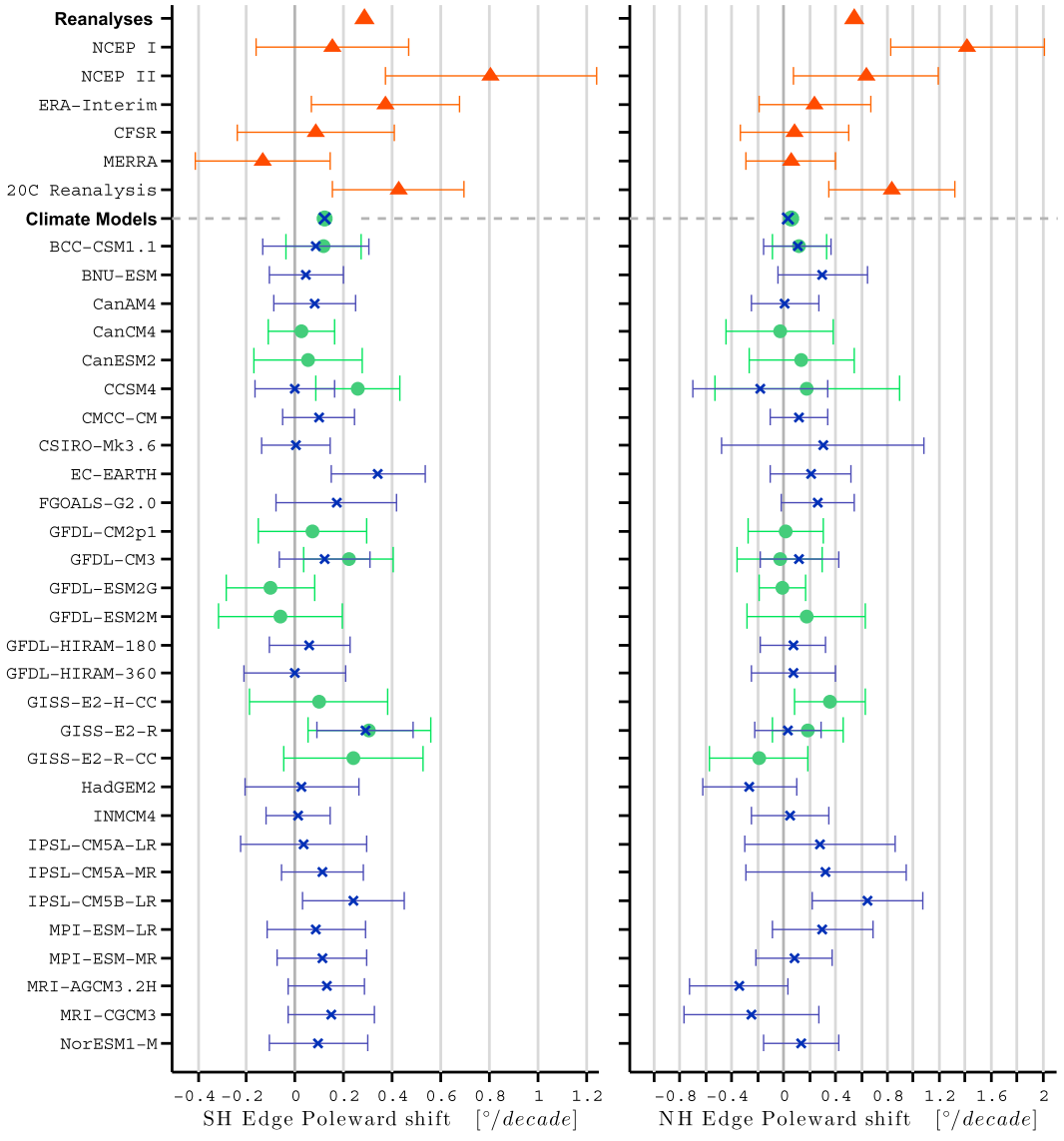

FIG. 4. Trends in poleward shift of HC terminus (°decade^{-1}) in the (left) Southern Hemisphere and (right) Northern Hemisphere during 1979–2005 for reanalyses (orange triangles), AMIP simulations (blue crosses), and CMIP5 simulations (green dots). Error bars show Studentized 95% confidence bounds. Ensemble means are shown as the respective symbol without error bars.

CFSR, and MERRA) show no statistically significant sensitivity to Mean(SST). Most climate simulations exhibit a sensitivity to Mean(SST) similar to that found for the ERA-Interim, CFSR, and MERRA reanalyses, with only 4 of the 33 AMIP and CMIP simulations showing a statistically significant positive sensitivity to Mean(SST).

All reanalyses exhibit a statistically significant positive sensitivity to Grad(SST). Similarly, 26 of the 33 climate simulations show a statistically significant positive sensitivity to Grad(SST). On average, the sensitivities of the ERA-Interim, CFSR, and MERRA reanalyses (~4.5° K^{-1}) are smaller than those found for the NCEP I, NCEP II, and 20C reanalyses (~8.5° K^{-1}), and are closer to those found in the AMIP and CMIP5 simulations (~3° K^{-1}).

Figure 6 shows the relative contributions of Mean(SST) (green) and Grad(SST) (blue) to the observed HCW changes (orange) during the entire period over which reliable data are available (1979–2012; Fig. 6a), and restricted to subperiods: 1979–97 (Fig. 6b), and 1997–2012 (Fig. 6c). The relative contributions are calculated by multiplying the changes in Grad(SST) and Mean (SST) during the given periods by a_1 and a_2, respectively. On average, the regression model captures 98% of the total HCW change for the period 1979–2012

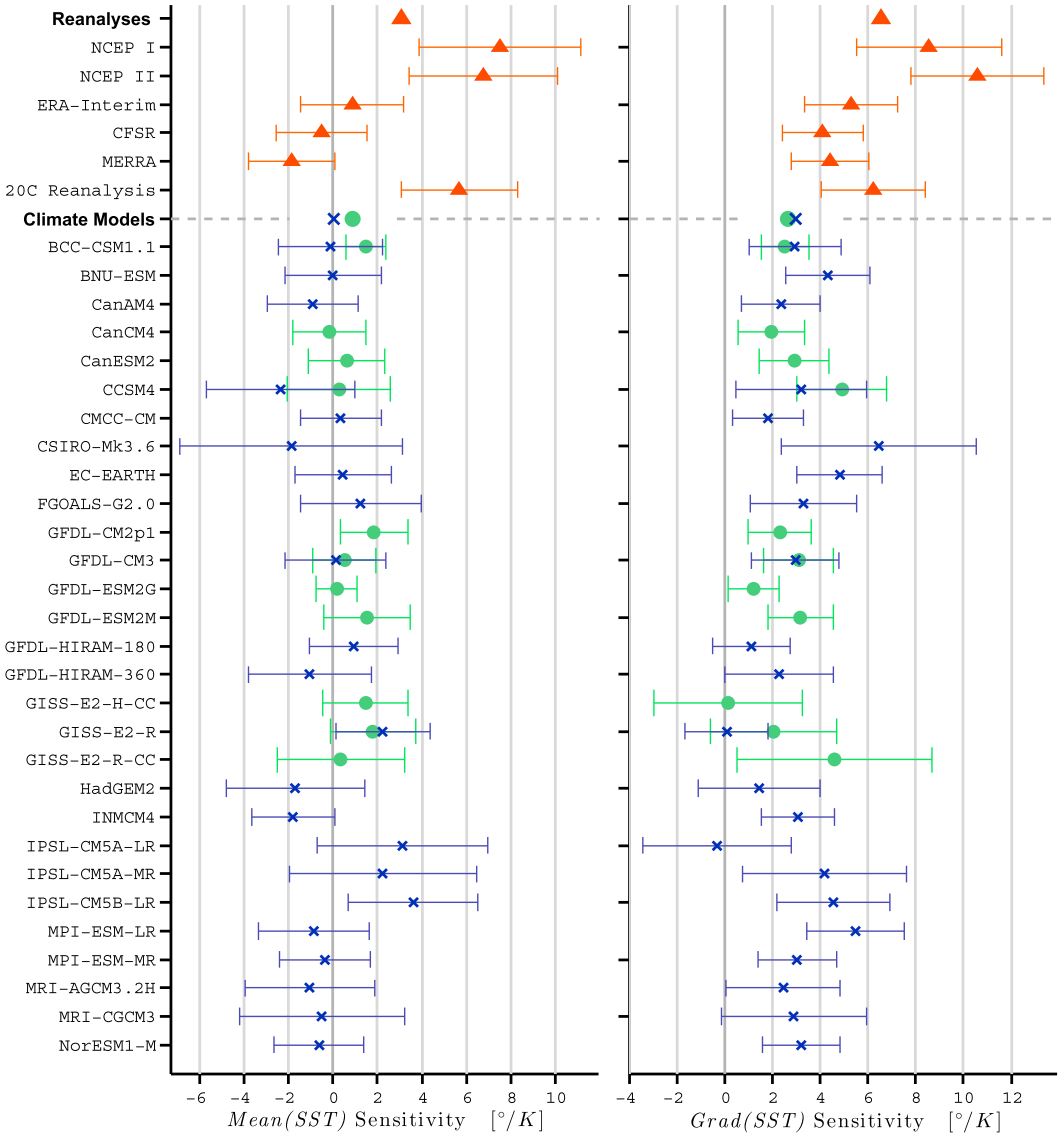

FIG. 5. HCW sensitivity to variations in (left) Mean(SST) and (right) Grad(SST), for reanalyses (orange triangles), AMIP simulations (blue crosses), and CMIP5 simulations (green dots). Error bars show Studentized 95% confidence bounds. Ensemble means are shown as the respective symbol without error bars. The periods used for the calculation of the sensitivities are 1979–2012, 1979–2008, and 1979–2005 for reanalyses, AMIP simulations, and CMIP5 simulations, respectively (with the exception of 1979–2011 for the 20C Reanalysis).

but much less for the shorter subperiods. The error margins per reanalysis and simulation ensemble are large, relative to the observed change in HCW. However, the consistency across reanalyses and simulations suggests that the regression model captures the key contributions to changes in HCW.

Both Mean(SST) and Grad(SST) changes contribute to the HCW change from 1979 to 2012 in different proportion for different reanalyses and simulations. For the subperiods, the regression analysis shows that the observed HC widening from 1979 to 1997 was dominated by an increase in Mean(SST). By contrast, the more recent HC widening from 1997 to 2012, during the global warming hiatus, is dominated by an increase in Grad(SST) (i.e., more prevalent La Niña conditions). Because the sensitivity of HCW to Mean(SST) is low in AMIP simulations, nearly all of the HCW changes in AMIP simulations are attributable to Grad(SST). In contrast, variations in Grad(SST) tend to cancel out when averaged in CMIP5 simulations (because the SST is not observationally constrained so that ENSO events are not in phase with observations or among simulations).

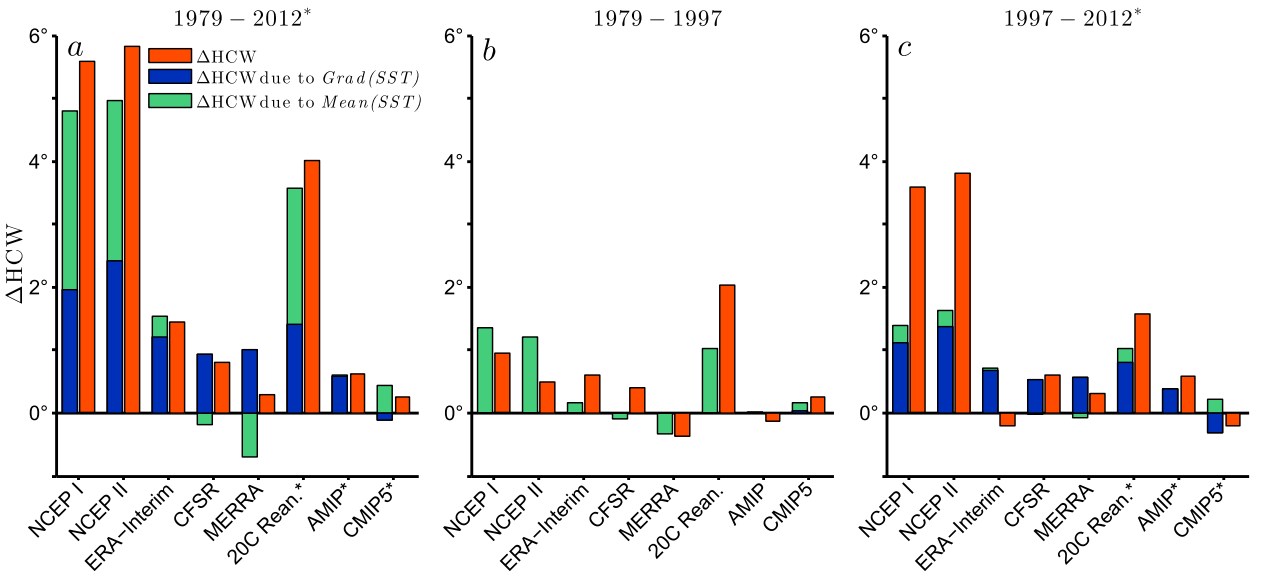

FIG. 6. Mean change in HCW (orange) and the respective change due to variations in Mean(SST) (green) and Grad(SST) (blue) in the six reanalyses, and in the AMIP and CMIP5 simulations (ensemble means). (a) Changes over 1979–2012 for reanalyses (1979–2011 for 20C Reanalysis), over 1979–2008 for AMIP simulations, and over 1979–2005 for CMIP5 simulations. (b) As in (a), but changes restricted to 1979–97. (c) As in (a), but changes restricted to 1997–2012 for reanalyses (1997–2011 for 20C Reanalysis), to 1997–2008 for AMIP simulations, and to 1997–2005 for CMIP5 simulations. The mean Studentized 95% confidence error bounds are (a) ±1.4°, (b) ±1.7°, and (c) ±2°.

Therefore most HCW changes in CMIP5 simulations are attributable to Mean(SST).

4. Discussion and conclusions

As already noted in previous studies, we found that the Hadley circulation generally widens when surface temperatures increase on large scales, as they do under global warming, and when temperature contrasts between the tropics and midlatitudes decrease, as they do under La Niña (e.g., Lu et al. 2007, 2008; Frierson et al. 2007; Levine and Schneider 2011; Nguyen et al. 2013). One way of interpreting these results, at least qualitatively, is that the HC terminates at the lowest latitude at which baroclinic eddies become sufficiently deep to reach the upper troposphere, leading to wave activity divergence poleward of that latitude and thus to upper-tropospheric equatorward flow balancing the resulting angular momentum flux convergence there (Korty and Schneider 2008). Relating the transition latitude to scaling theories for the depth of baroclinic eddies (Held 1978; Schneider and Walker 2006) leads to the expectation that the HC extends to where the isentropic slope first exceeds a critical value (Korty and Schneider 2008; see also, Held 2000; Walker and Schneider 2006; Lu et al. 2007). Because the isentropic slope is a ratio of a meridional temperature gradient and a static stability, the HC is expected to widen as subtropical meridional temperature gradients weaken (as under La Niña) and/or as the static stability increases (as under global warming, because the dry static stability of a moist adiabat increases as the temperature increases). Making these qualitative mechanistic statements quantitative and testing them requires further study.

What we can conclude empirically and quantitatively is that variations in large-scale mean SST [Mean(SST)] and in midlatitude-to-tropics SST gradients [Grad(SST)] account for about two-thirds of the interannual HCW variations over the years 1979–2012 in six reanalyses. They account for a similar portion of interannual HCW variations in 22 AMIP and 11 CMIP5 simulations spanning the years 1979–2008 and 1979–2005, respectively. However, HCW sensitivities to variations in these indices differ substantially among reanalyses and climate models, and the statistical significance of trends and sensitivities is limited.

Regressing HCW variations on Mean(SST) and Grad(SST) suggests that the HC widening over the years 1979–97 is primarily associated with global warming. By contrast, the continued HC widening from 1997 to 2012 is mostly associated with Grad(SST) changes, consistent with reduced tropics-to-midlatitude temperature contrasts, such as occur under La Niña. More detailed analysis (Fig. 7) reveals that the primary contributor to these

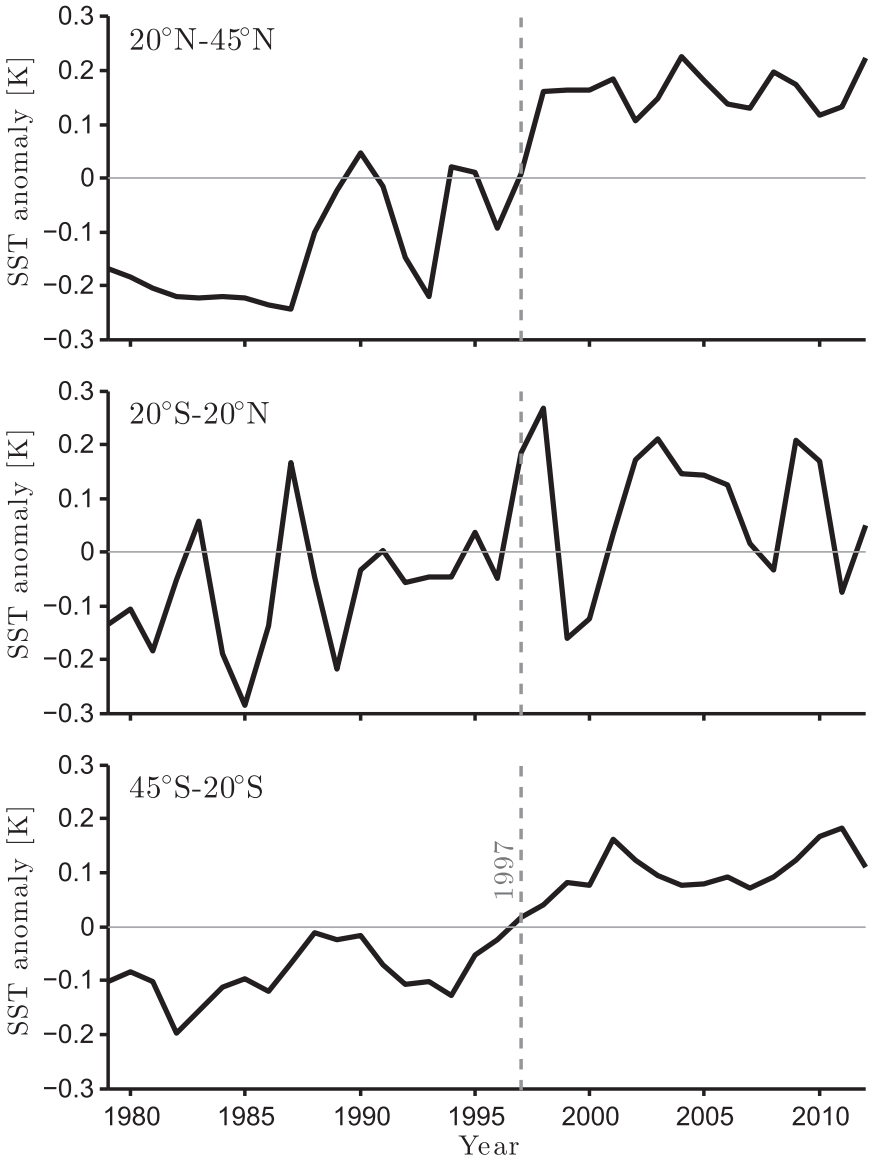

FIG. 7. Time series of the zonally and annually averaged SST anomaly (ERSST) during 1979–2012 in the latitude bands (top) 20°–45°N, (middle) 20°S–20°N, and (bottom) 45°–20°S.

Grad(SST) changes is elevated midlatitude SSTs (especially in the Pacific) while tropical SSTs increase less. This is consistent with recent theoretical and observational studies that suggest the global warming hiatus is related to increased tropical deep ocean heat uptake brought about by more prevalent La Niña conditions while temperatures in the North Pacific are elevated (Meehl et al. 2011; Balmaseda et al. 2013; Kosaka and Xie 2013; Allen et al. 2014). However, while these results are not sensitive to the choice of 1997 as the year for subdividing the record—choosing 1996 or 1998 as the subdivision year yields similar results—they vary considerably among reanalyses.

The large spread of HCW variations across reanalyses precludes a clear determination of the level of agreement between observed and simulated HCW trends (Quan et al. 2014; Davis and Rosenlof 2012). The latest-generation ERA-Interim, CFSR, and MERRA reanalyses display similar HCW trends and sensitivity to variations in Mean (SST) and Grad(SST) as the climate models. On the other hand, the older-generation NCEP I and NCEP II reanalyses, as well as the 20C Reanalysis, display significantly larger trends and sensitivity to variations in these indices.

Ozone depletion may also play an important role in the HC widening, in particular at the Southern Hemisphere (Polvani and Kushner 2002; Polvani

et al. 2011). However, as shown here, the majority of the widening can be accounted for by SST variations, which are, at most, very weakly affected by ozone depletion.

Acknowledgments. This research was supported by the U.S. National Science Foundation (Grant AGS-1049201) and Israeli Science Foundation Grant 1537/12. All calculations presented here were performed using the Geophysical Observation Analysis Tool (GOAT), a freely available MATLAB-based tool for retrieval, analysis, and visualization of geophysical data (http://www.goat-geo.org).

REFERENCES

Allen, R. J., J. R. Norris, and M. Kovilakam, 2014: Influence of anthropogenic aerosols and the Pacific Decadal Oscillation on tropical belt width. *Nat. Geosci.,* **7,** 270–274, doi:10.1038/ngeo2091.

Balmaseda, M. A., K. E. Trenberth, and E. Källén, 2013: Distinctive climate signals in reanalysis of global ocean heat content. *Geophys. Res. Lett.,* **40,** 1754–1759, doi:10.1002/grl.50382.

Ceppi, P., and D. Hartmann, 2013: On the speed of the eddy-driven jet and the width of the Hadley cell in the Southern Hemisphere. *J. Climate,* **26,** 3450–3465, doi:10.1175/JCLI-D-12-00414.1.

Compo, G. P., and Coauthors, 2011: The Twentieth Century Reanalysis project. *Quart. J. Roy. Meteor. Soc.,* **137,** 1–28, doi:10.1002/qj.776.

Cubasch, U., and Coauthors, 2013: Introduction. *Climate Change 2013: The Physical Science Basis,* T. F. Stocker, et al., Eds., Cambridge University Press, 119–158. [Available online at http://www.climatechange2013.org/images/report/WG1AR5_Chapter01_FINAL.pdf.]

Davis, N. A., and T. Birner, 2013: Seasonal to multidecadal variability of the width of the tropical belt. *J. Geophys. Res.,* **118,** 7773–7787, doi:10.1002/jgrd.50610.

Davis, S. M., and K. H. Rosenlof, 2012: A multidiagnostic intercomparison of tropical-width time series using reanalyses and satellite observations. *J. Climate,* **25,** 1061–1078, doi:10.1175/JCLI-D-11-00127.1.

Dee, D. P., and Coauthors, 2011: The ERA-Interim Reanalysis: Configuration and performance of the data assimilation system. *Quart. J. Roy. Meteor. Soc.,* **137,** 553–597, doi:10.1002/qj.828.

Frierson, D. M. W., J. Lu, and G. Chen, 2007: Width of the Hadley cell in simple and comprehensive general circulation models. *Geophys. Res. Lett.,* **34,** L18804, doi:10.1029/2007GL031115.

Hansen, J. E., and S. Lebedeff, 1987: Global trends of measured surface air temperature. *J. Geophys. Res.,* **92,** 13 345–13 372, doi:10.1029/JD092iD11p13345.

Held, I. M., 1978: The vertical scale of an unstable baroclinic wave and its importance for eddy heat flux parameterizations. *J. Atmos. Sci.,* **35,** 572–576, doi:10.1175/1520-0469(1978)035<0572:TVSOAU>2.0.CO;2.

——, 2000: The general circulation of the atmosphere. [Available online at http://www.gfdl.noaa.gov/cms-filesystem-action/user_files/ih/lectures/woods_hole.pdf.]

Hu, Y., and Q. Fu, 2007: Observed poleward expansion of the Hadley circulation since 1979. *Atmos. Chem. Phys.,* **7,** 5229–5236, doi:10.5194/acp-7-5229-2007.

Johanson, C. M., and Q. Fu, 2009: Hadley cell widening: Model simulations versus observations. *J. Climate,* **22,** 2713–2725, doi:10.1175/2008JCLI2620.1.

Kalnay, E., and Coauthors, 1996: The NCEP/NCAR 40-Year Reanalysis Project. *Bull. Amer. Meteor. Soc.,* **77,** 437–471, doi:10.1175/1520-0477(1996)077<0437:TNYRP>2.0.CO;2.

Kanamitsu, M., and Coauthors, 2002: NCEP dynamical seasonal forecast system 2000. *Bull. Amer. Meteor. Soc.,* **83,** 1019–1037, doi:10.1175/1520-0477(2002)083<1019:NDSFS>2.3.CO;2.

Kang, S. M., and J. Lu, 2012: Expansion of the Hadley cell under global warming: Winter versus summer. *J. Climate,* **25,** 8387–8393, doi:10.1175/JCLI-D-12-00323.1.

——, C. Deser, and L. M. Polvani, 2013: Uncertainty in climate change projections of the Hadley circulation: The role of internal variability. *J. Climate,* **26,** 7541–7554, doi:10.1175/JCLI-D-12-00788.1.

Korty, R. L., and T. Schneider, 2008: Extent of Hadley circulations in dry atmospheres. *Geophys. Res. Lett.,* **35,** L23803, doi:10.1029/2008GL035847.

Kosaka, Y., and S.-P. Xie, 2013: Recent global-warming hiatus tied to equatorial Pacific surface cooling. *Nature,* **501,** 403–407, doi:10.1038/nature12534.

Levine, X. J., and T. Schneider, 2011: Response of the Hadley circulation to climate change in an aquaplanet GCM coupled to a simple representation of ocean heat transport. *J. Atmos. Sci.,* **68,** 769–783, doi:10.1175/2010JAS3553.1.

Lu, J., G. A. Vecchi, and T. Reichler, 2007: Expansion of the Hadley cell under global warming. *Geophys. Res. Lett.,* **34,** L06805, doi:10.1029/2006GL028443.

——, G. Chen, and D. M. W. Frierson, 2008: Response of the zonal mean atmospheric circulation to El Niño versus global warming. *J. Climate,* **21,** 5835–5851, doi:10.1175/2008JCLI2200.1.

Lucas, C., B. Timbal, and H. Nguyen, 2014: The expanding tropics: A critical assessment of the observational and modeling studies. *Wiley Interdiscip. Rev.: Climate Change,* **5,** 89–112, doi:10.1002/wcc.251.

Meehl, G. A., J. Arblaster, J. Fasullo, A. Hu, and K. Trenberth, 2011: Model-based evidence of deep-ocean heat uptake during surface-temperature hiatus periods. *Nat. Climate Change,* **1,** 360–364, doi:10.1038/nclimate1229.

Nguyen, H., A. Evans, C. Lucas, I. Smith, and B. Timbal, 2013: The Hadley circulation in reanalyses: Climatology, variability, and change. *J. Climate,* **26,** 3357–3376, doi:10.1175/JCLI-D-12-00224.1.

Polvani, L. M., and P. J. Kushner, 2002: Tropospheric response to stratospheric perturbations in a relatively simple general circulation model. *Geophys. Res. Lett.,* **29,** 1114, doi:10.1029/2001GL014284.

——, D. W. Waugh, G. J. P. Correa, and S.-W. Son, 2011: Stratospheric ozone depletion: The main driver of twentieth-century atmospheric circulation changes in the Southern Hemisphere. *J. Climate,* **24,** 795–812, doi:10.1175/2010JCLI3772.1.

Quan, X.-W., M. Hoerling, J. Perlwitz, H. Diaz, and T. Xu, 2014: How fast are the tropics expanding? *J. Climate,* **27,** 1999–2013, doi:10.1175/JCLI-D-13-00287.1.

Rienecker, M. M., and Coauthors, 2011: MERRA: NASA's Modern-Era Retrospective Analysis for Research and Applications. *J. Climate,* **24,** 3624–3648, doi:10.1175/JCLI-D-11-00015.1.

Saha, S., and Coauthors, 2010: The NCEP Climate Forecast System Reanalysis. *Bull. Amer. Meteor. Soc.,* **91,** 1015–1057, doi:10.1175/2010BAMS3001.1.

Schneider, T., and C. C. Walker, 2006: Self-organization of atmospheric macroturbulence into critical states of weak nonlinear eddy–eddy interactions. *J. Atmos. Sci.,* **63,** 1569–1586, doi:10.1175/JAS3699.1.

Seager, R., N. Harnik, Y. Kushnir, W. Robinson, and J. Miller, 2003: Mechanisms of hemispherically symmetric climate variability. *J. Climate,* **16,** 2960–2978, doi:10.1175/1520-0442(2003)016<2960:MOHSCV>2.0.CO;2.

Seidel, D. J., and W. J. Randel, 2007: Recent widening of the tropical belt: Evidence from tropopause observations. *J. Geophys. Res.,* **112,** D20113, doi:10.1029/2007JD008861.

Smith, T. M., R. W. Reynolds, T. C. Peterson, and J. Lawrimore, 2008: Improvements to NOAA's historical merged land–ocean surface temperature analysis (1880–2006). *J. Climate,* **21,** 2283–2296, doi:10.1175/2007JCLI2100.1.

Walker, C. C., and T. Schneider, 2006: Eddy influences on Hadley circulations: Simulations with an idealized GCM. *J. Atmos. Sci.,* **63,** 3333–3350, doi:10.1175/JAS3821.1.